INSTITUT DE FRANCE
Académie des sciences

Comptes Rendus
Mécanique

Nicolas Moës and Nicolas Chevaugeon

Lipschitz regularization for softening material models: the Lip-field approach

Volume 349, issue 2 (2021), p. 415-434

Published online: 9 August 2021

https://doi.org/10.5802/crmeca.91

Les Comptes Rendus. Mécanique *sont membres du Centre Mersenne pour l'édition scientifique ouverte*
www.centre-mersenne.org
e-ISSN : 1873-7234

Comptes Rendus
Mécanique
2021, 349, nº 2, p. 415-434
https://doi.org/10.5802/crmeca.91

Short paper / *Note*

Lipschitz regularization for softening material models: the Lip-field approach

Régularisation de Lipschitz pour les modèles de matériaux adoucissants : l'approche Lip-field

Nicolas Moës [*, a, b] **and Nicolas Chevaugeon** [a]

[a] Ecole Centrale de Nantes, GeM Institute, UMR CNRS 6183, 1 rue de la Noë, 44321 Nantes, France

[b] Institut Universitaire de France (IUF), France

E-mails: nicolas.moes@ec-nantes.fr (N. Moës), nicolas.chevaugeon@ec-nantes.fr (N. Chevaugeon)

Abstract. Softening material models are known to trigger spurious localizations. This may be shown theoretically by the existence of solutions with zero dissipation when localization occurs and numerically with spurious mesh dependency and localization in a single layer of elements. We introduce in this paper a new way to avoid spurious localization. The idea is to enforce a Lipschitz regularity on the internal variables responsible for the material softening. The regularity constraint introduces the needed length scale in the material formulation. Moreover, we prove bounds on the domain affected by this constraint. A first one-dimensional finite element implementation is proposed for softening elasticity and softening plasticity.

Résumé. Les modèles de matériaux adoucissants sont connus pour déclencher des localisations parasites. Cela peut être démontré théoriquement par l'existence de solutions avec une dissipation nulle lors de la localisation et numériquement avec une dépendance de maillage et une localisation dans une seule couche d'éléments. Nous introduisons dans cet article une nouvelle façon d'éviter les localisations parasites. L'idée est d'imposer une régularité de Lipschitz sur les variables internes responsables de l'adoucissement. La contrainte de régularité introduit l'échelle de longueur nécessaire dans la formulation du matériau. De plus, nous prouvons des bornes sur le domaine affecté par cette contrainte. Une première mise en œuvre par éléments finis unidimensionnels est proposée pour l'adoucissement élastique ou plastique.

Keywords. Softening, Localization, Damage, Plasticity, Lipschitz, Lip-field.

Mots-clés. Adoucissement, Localisation, Endommagement, Plasticité, Lipschitz, Lip-field.

Manuscript received 30th March 2021, revised 14th May 2021, accepted 19th July 2021.

* Corresponding author.

1. Introduction

With softening, the stress that a material can sustain is diminishing as the strain increases. This phenomenon exists both for elasticity and plasticity. For elasticity, the stiffness is decreasing as the strain increases, whereas for plasticity, the yield stress is diminishing as the plastic strain accumulates. Dealing with these types of models in finite element analysis is a challenge. From the mathematical point of view, these models loose the nice convex properties of classical elastic models or hardening plasticity models. Limit points may exist: the solution does not exist beyond some loads. Bifurcation points are also possible: at some stage in time, several solutions start to exist (stable or not). Among the many solutions that may exist, some are called spurious localizations. In the one-dimensional (1D) setting, these localizations are characterized by a softening occurring in a single point. For higher dimensions, the localization occurs on zero-measure domains. As a consequence, the dissipation involved in these zones is zero. In other words, the external energy or load needed to diminish the bearing capacity of the structure is highly underestimated. The mathematical difficulties of softening material models have a direct impact on their numerical treatment. Spurious mesh dependency is observed with finite elements: the mesh orientation has a strong impact on the results and, as the mesh is refined, only a single element, or a layer of elements, depending on the problem dimension, is affected by localization.

This paper introduces a new way to eliminate these spurious localizations from the model. It does not mean that the solution is now unique but, at least these unwanted solutions are removed. The design of approaches to remove spurious localizations has been going on for about forty years now.

Regarding quasi-static analysis of time-independent models, several remedies have been studied in the literature. They all share in common the fact that a regularizing length scale is injected in the model. For the so-called non-local integral damage model, the damage evolution at a given point is governed by a driving force which is the average of the local driving force over some distance around that point [1–4]. Refinements of the non-local integral model with an evolving internal length may be found in [5, 6].

In higher order, kinematically based gradient models, the length scale is introduced through the inclusion of higher order deformation gradient in the energy expression [7–9] or through additional rotational degrees of freedom [10]. For higher order, damage-based gradient models, the energy depends on the gradient of the damage thus involving again a length scale [11–14].

Regarding the energy minimizing approaches, they mainly stem from the seminal paper by Mumford and Shah [15]. The Italian school of calculus of variations has given most of the mathematical background for models of brittle fracture based on the Mumford–Shah function [16, 17] and the variational approximations [18]. In a very early paper, which uses minimizing movements [19] and variational approximations is [20], and in [21], the Ambrosio Tortorelli approximation is used for a damage energy minimizing model, which turned out to be related mathematically with viscosity-based approaches to introduce a length scale into damage. The Ambrosio Tortorelli approximation was also used by Bourdin *et al.* [22] to implement the revisit of brittle fracture introduced in [23], leading to the so-called variational approach to fracture [24, 25].

At about the same time, the phase-field approach was emanating from the physics community [26, 27] and then developed for mechanics applications [28–32].

Yet another way to introduce a length scale is the thick level set approach to fracture. The approach was introduced for brittle damage in [33, 34]. The damage evolution is tied to a distance field. The damage front on which the damage starts is the level set zero and it grows to a value of 1 (fully damage state) at some distance l_c in the wake of the front. That amounts to imposing the norm of the damage gradient on zones with strictly positive damage (equality constraint).

The possibility of an inequality constraint on the damage gradient was also considered in [35,36] allowing to combine diffuse and localizing damage fields. The advantage of this inequality was further stressed in [37], where it was shown that the inequality constraint is convex on the contrary to the equality constraint. This paper also demonstrates that a level set field is not mandatory: a variational approach with Lagrange multipliers enforcing the inequality constraint may be used. Following the ideas of [37], an implementation is provided in [38].

The Lipschitz regularization introduced in this paper enforces a regularity on the damage field. The obtained field is called a Lip-field. The Lipschitz regularity does not require the existence of the damage gradient. Yet, the Lip-field is differentiable almost everywhere. To present the Lip-field concept, the appealing framework of incremental energetic variational potential is considered. The interest of this framework was first demonstrated for visco-plasticity [39,40] and was later reused as a building block for the variational approach to fracture [25]. When softening may occur, the incremental potential is not convex but only separately convex with respect to the displacement (and non-softening internal variable) on one side and softening variable on the other side. It is thus natural to proceed with an alternate minimization of successive convex problems [41]. The Lip-field convex constraint is added as an extra constraint in the alternate minimization. We demonstrate in this paper upper and lower bounds for the minimization over the damage field. These bounds reduce drastically the zone over which the Lipschitz condition needs to be activated. The proof holds in any spatial dimension.

A 1D finite element implementation is provided for the Lip-field approach. The potential needs to be minimized for the nodal values of the displacement and for the internal variables located at the integration point in each finite element, including the damage state variable. In other words, with the Lip-field approach, the damage variable may be kept at the integration points with the other internal variables and does not need to be stored at the nodes, thus following the common practice for nonlinear finite element analysis.

Finally, note that there is also current interest in Lipschitz regularization to improve the robustness to adversarial perturbations for learning framework [42].

The paper is organized as follows. The next section describes the classical mechanical formulation for non-softening material models. In Section 3, a softening variable is introduced, and the Lipschitz constraint is imposed. Elastic and plastic softening models are presented in Section 4 for the 1D setting. Finite element analyses are carried out in Section 5. Discussion and future works are provided in Section 6.

2. Generalized standard materials

We consider the deformation of a body initially occupying a domain Ω through a displacement field $\boldsymbol{u}$. For simplicity, we assume small, quasi-static deformations. The Cauchy stress is denoted by $\boldsymbol{\sigma}$ and the strain by $\boldsymbol{\epsilon}$

$$\boldsymbol{\epsilon}(\boldsymbol{u}) = \tfrac{1}{2}(\nabla \boldsymbol{u} + (\nabla \boldsymbol{u})^{\mathrm{T}}), \tag{1}$$

where ∇ indicates the gradient operator. Regarding the boundary conditions, the displacement is controlled on a part of the boundary denoted by Γ_u assumed fixed in time. On the rest of boundary, zero traction force is assumed (again for simplicity). To be kinematically admissible at some instant t, the displacement field must belong to $U(t)$:

$$U(t) = \{\boldsymbol{u} \in H^1(\Omega) : \boldsymbol{u} = \boldsymbol{u}_d(t) \text{ on } \Gamma_u\}. \tag{2}$$

The equilibrium condition reads

$$\int_\Omega \boldsymbol{\sigma} : \boldsymbol{\epsilon}(\boldsymbol{u}^*)\, \mathrm{d}\Omega = 0, \quad \forall \boldsymbol{u}^* \in U^*, \tag{3}$$

where

$$U^* = \{\boldsymbol{u} \in H^1(\Omega) : \boldsymbol{u} = 0 \text{ on } \Gamma_u\}. \tag{4}$$

Kinematics and equilibrium equations (2)–(3) must be complemented with the constitutive model. We consider the formalism of generalized standard material introduced in [43, 44]. The set of internal variables is denoted by α. It is a generic notation that describes a set of scalar, vectorial, or tensorial variables. The model is characterized by a free energy potential $\varphi(\boldsymbol{\epsilon}, \alpha)$ and a dissipation potential $\psi(\dot{\alpha}, \alpha)$. We then introduce an implicit time discretization and use the energetic variational approach. Consider the displacement and internal variables $(\boldsymbol{u}_n, \alpha_n)$ known at some instant t_n. Finding the pair $(\boldsymbol{u}_{n+1}, \alpha_{n+1})$ at the next instant $t_{n+1} = t_n + \Delta t$ amounts to a minimization problem

$$(\boldsymbol{u}_{n+1}, \alpha_{n+1}) = \arg \min_{\substack{\boldsymbol{u}' \in U_n \\ \alpha' \in A_n}} F(\boldsymbol{u}', \alpha'; \boldsymbol{u}_n, \alpha_n, \Delta t), \tag{5}$$

where U_n is a short-hand notation for $U(t_{n+1})$ and A_n indicates the restriction on α_{n+1}. The incremental potential F involves the energy and dissipation potentials φ and ψ. Examples of incremental potentials will be given in Section 4.

For simplicity, we shall consider time-independent material models. In this case, the F expression does not depend explicitly on $\boldsymbol{u}_n, \alpha_n$, and Δt. The extension to time-dependent models does not introduce difficulties. Also, to lighten notation, we drop the $n+1$ indices. The minimization problem is then

$$(\boldsymbol{u}, \alpha) = \arg \min_{\substack{\boldsymbol{u}' \in U_n \\ \alpha' \in A_n}} F(\boldsymbol{u}', \alpha'). \tag{6}$$

We assume that the domains U_n and A_n are convex and that F is strictly convex with respect to the pair $(\boldsymbol{u}, \alpha)$ over $U_n \times A_n$. This defines a non-softening model. The minimization is traditionally solved by a repeated sequence of two steps: the computation of the internal variables (and stress) for a given displacement field, followed by the correction of the displacement field. At iteration m, the two steps are given below

$$\alpha^{m+1} = \arg \min_{\alpha \in A_n} F(\boldsymbol{u}^m, \alpha) \tag{7}$$

$$\{\boldsymbol{u}^{m+1}\} = \{\boldsymbol{u}^m\} + (K^m)^{-1} R^m, \quad \boldsymbol{u}^{m+1} \in U_n. \tag{8}$$

The first step, Equation (7), is purely local and may be carried out independently at each material point. The second step, Equation (8), involves a linear solve which updates the degrees of freedom $\{\boldsymbol{u}\}$ associated to the field $\boldsymbol{u}$. The matrix K depends on the current internal variables α^{m+1}, and the residual vector R depends on the current stress $\boldsymbol{\sigma}^{m+1}$. The matrix can be the algorithmic tangent operator [45] or some approximation of it. The linear solver may possibly be followed by a line search to further improve the solution. Expressions of K and R are given in the Appendix B for the models at stake in this paper.

3. Softening variable and Lipschitz regularization

We now consider that the model has an extra scalar variable d responsible for softening. The optimization problem becomes

$$(\boldsymbol{u}, \alpha, d) = \arg \min_{\substack{(\boldsymbol{u}', \alpha') \in U_n \times A_n \\ d' \in D_n}} F(\boldsymbol{u}', \alpha', d'). \tag{9}$$

It is no longer convex, we can expect several local minima and also non-uniqueness to the global minimum (i.e., several solutions leading to the same global minimum). Even though F is not convex with respect to the triple $(\boldsymbol{u}, \alpha, d)$, we ask the optimization to be convex with respect to the couple $(\boldsymbol{u}, \alpha)$ for all $d \in D_n$ and to be convex with respect to d for all $(\boldsymbol{u}, \alpha) \in U_n \times A_n$.

Given a d field over the domain Ω, the Lipschitz constant associated to this field is the minimum M value such that the following holds

$$|d(\boldsymbol{x}) - d(\boldsymbol{y})| \leq M \operatorname{dist}(\boldsymbol{x}, \boldsymbol{y}), \quad \forall \boldsymbol{x}, \boldsymbol{y} \in \Omega, \tag{10}$$

where $\operatorname{dist}(\boldsymbol{x}, \boldsymbol{y})$ is the minimal length of the path inside Ω joining $\boldsymbol{x}$ and $\boldsymbol{y}$ (the distance is considered infinite if the two points cannot be connected inside Ω). The dist function is a metric since it satisfies for all $\boldsymbol{x}, \boldsymbol{y}, \boldsymbol{z} \in \Omega$:

$$\operatorname{dist}(\boldsymbol{x}, \boldsymbol{y}) = 0 \Leftrightarrow \boldsymbol{x} = \boldsymbol{y} \tag{11}$$

$$\operatorname{dist}(\boldsymbol{x}, \boldsymbol{y}) = \operatorname{dist}(\boldsymbol{y}, \boldsymbol{x}) \tag{12}$$

$$\operatorname{dist}(\boldsymbol{x}, \boldsymbol{y}) \leq \operatorname{dist}(\boldsymbol{x}, \boldsymbol{z}) + \operatorname{dist}(\boldsymbol{z}, \boldsymbol{y}). \tag{13}$$

The value M defined above is denoted by $\operatorname{lip}(d)$. We define the regularization space for the damage field

$$L = \{d \in L^\infty(\Omega) : \operatorname{lip}(d) \leq 1/l\}, \tag{14}$$

where l is the regularizing length. The set L is convex. We seek the solution as "one" of the global minima

$$(\boldsymbol{u}, \alpha, d) = \arg \min_{\substack{(\boldsymbol{u}', \alpha') \in U_n \times A_n \\ d' \in D_n \cap L}} F(\boldsymbol{u}', \alpha', d'). \tag{15}$$

We proceed by alternate minimization

$$(\boldsymbol{u}^{k+1}, \alpha^{k+1}) = \arg \min_{(\boldsymbol{u}, \alpha) \in U_n \times A_n} F(\boldsymbol{u}, \alpha, d^k) \tag{16}$$

$$d^{k+1} = \arg \min_{d \in D_n \cap L} F(\boldsymbol{u}^{k+1}, \alpha^{k+1}, d). \tag{17}$$

For the first minimization, the damage variable is frozen and the problem is thus identical to problem (6). It is a classical non-softening step. The second minimization, Equation (17), is less common. The objective function is convex (and separable) as well as the constraint D_n. The Lip constraint is non-local as it ties the damage variables between points. The optimization to find d is thus potentially time-consuming when turning to a numerical implementation. The good news is that the quest for d may be decomposed into three steps reducing dramatically the cost of the optimization. The first step is to create a trial d field denoted $\overline{d}$ by ignoring the Lipschitz constraint and performing a decoupled minimization at each point

$$\overline{d} = \arg \min_{d \in D_n} F(\boldsymbol{u}^{k+1}, \alpha^{k+1}, d). \tag{18}$$

If the trial damage $\overline{d}$ satisfies the Lipschitz constraint, it is the solution we are looking for as indicated in Figure 1 (left). If not, the optimal damage field will be different from $\overline{d}$.

We can find an upper bound of the domain over which d^{k+1} will differ from $\overline{d}$. We define two projections onto L, a lower projection π^{l} and an upper projection π^{u}:

$$\pi^{\mathrm{l}}\overline{d}(\boldsymbol{x}) = \min_{\boldsymbol{y} \in \Omega} \left(\overline{d}(\boldsymbol{y}) + \frac{1}{l} \operatorname{dist}(\boldsymbol{x}, \boldsymbol{y}) \right) \tag{19}$$

$$\pi^{\mathrm{u}}\overline{d}(\boldsymbol{x}) = \max_{\boldsymbol{y} \in \Omega} \left(\overline{d}(\boldsymbol{y}) - \frac{1}{l} \operatorname{dist}(\boldsymbol{x}, \boldsymbol{y}) \right). \tag{20}$$

We prove in the Appendix A that these projections satisfy the following inequality

$$d_n \leq \pi^{\mathrm{l}}\overline{d} \leq \overline{d} \leq \pi^{\mathrm{u}}\overline{d} \leq 1 \tag{21}$$

and provide bounds for the optimal damage

$$\pi^{\mathrm{l}}\overline{d} \leq d^{k+1} \leq \pi^{\mathrm{u}}\overline{d}. \tag{22}$$

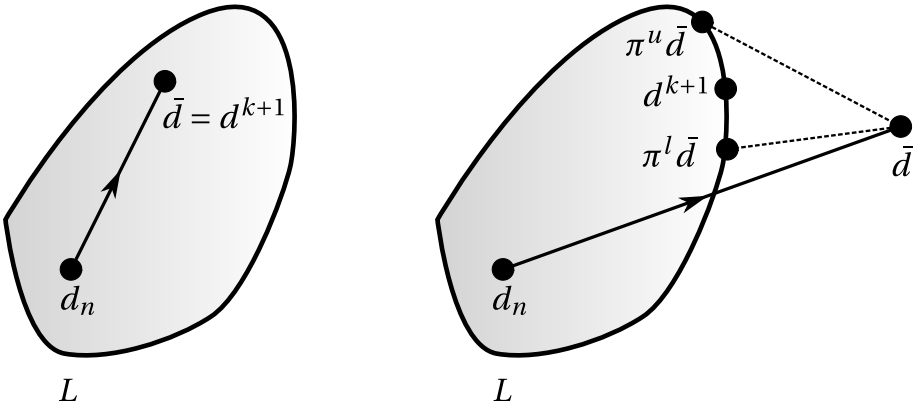

Figure 1. A sketch of the local update $\overline{d}$ from the previous known damage field d_n. If the update satisfies the Lip constraint (left), we have directly the solution d^{k+1}. Otherwise (right), the local update needs to be projected back to the Lip constraint while minimizing the objective function F. The upper and lower projections give bounds to the solution.

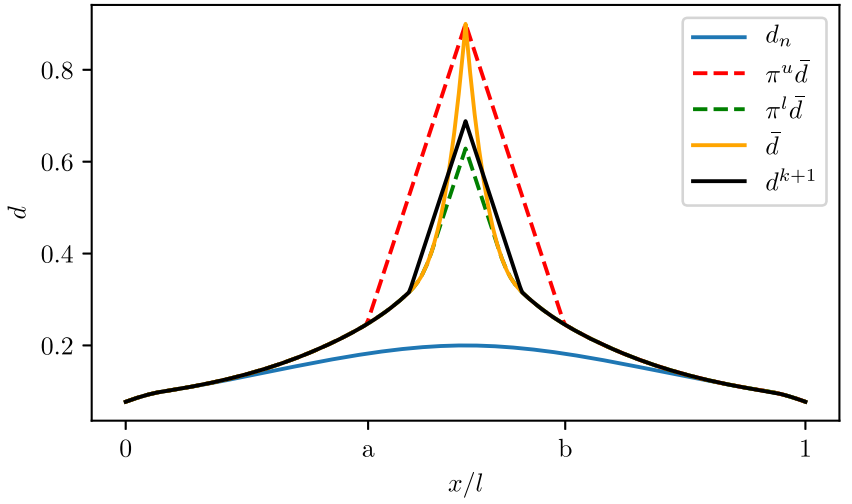

Figure 2. A sketch of the bracketing capability of the upper and lower projections. Outside the interval $[a, b]$, the projections are equal and thus $d^{k+1} = \overline{d}$. Inside the interval $[a, b]$, the projections bracket $\overline{d}$ and d^{k+1}.

As an important consequence, the trial and optimal solutions coincide wherever the bounds are equal

$$\pi^{\mathrm{l}}\overline{d}(\boldsymbol{x}) = \pi^{\mathrm{u}}\overline{d}(\boldsymbol{x}) \quad \Rightarrow \quad d^{k+1}(\boldsymbol{x}) = \overline{d}(\boldsymbol{x}). \tag{23}$$

A sketch of the projections is given in Figure 1 (right), and they are also illustrated on the 1D example, Figure 2.

4. Elastic and plastic softening models

Consider the 1D model of a bar of length L and unit section attached at its left side and pulled with an imposed displacement $u_d(t)$ at its right end. The displacement at time t must belong to

the set

$$U(t) = \{u \in C([0,L]) : u(0) = 0,\ u(L) = u_d(t)\},$$

whereas the set of admissible displacement variations is given by

$$U^* = \{u \in C([0,L]) : u(0) = 0,\ u(L) = 0\}.$$

We now detail several incremental potentials to be used in the simulation.

4.1. *Softening elasticity*

The elastic potential reads

$$F_{\mathrm{e}}(u) = \int_0^L f_e(\epsilon(u))\,\mathrm{d}x, \quad f_e(\epsilon(u)) = \frac{1}{2}E\epsilon(u)^2, \tag{24}$$

where $\epsilon(u) = \mathrm{d}u/\mathrm{d}x$ and E is the Young modulus. The elastic softening model, affects E and adds a dissipation term. For simplicity, we do not consider tension–compression dissymmetry in the model (the bar will always be in tension in the simulation). The softening elasticity potential is

$$F_{\mathrm{se}}(u,d) = \int_0^L f_{\mathrm{se}}(\epsilon(u),d)\,\mathrm{d}x, \quad f_{\mathrm{se}}(\epsilon(u),d) = (1-d)^2 f_e(\epsilon(u)) + Y_c h(d) \tag{25}$$

where Y_c is the critical energy release rate and the convex function $h(d)$ defines the softening behavior. Damage can only grow and cannot go beyond 1. The convex constraint set D_n for damage is

$$D_n = \{d \in L^\infty([0,L]) : d_n \le d \le 1\}. \tag{26}$$

The power 2 over the factor $(1-d)$ ensures convexity and a finite opening as $d \to 1$ [46]. Note that the proper choice of the power is also an issue with gradient damage models for which a value of 2 also ensures a finite opening [47]. We consider two choices for $h(d)$

$$h_1(d) = 2d + 3d^2 \tag{27}$$

$$h_2(d) = \frac{2d - d^2}{(1 - d + \lambda d^2)^2}. \tag{28}$$

Both functions are convex (provided $\lambda \le 1/2$). The condition $h'(0) = 2$ ensures that when damage starts $E\epsilon^2/2 = Y_c$. The second choice allows to mimic a linear cohesive-zone model [48], where λ is defined by

$$\lambda = 2\frac{Y_c l}{G_c} \tag{29}$$

with G_c denoting the toughness (energy per section area needed to break the bar). We shall see that the choice of $h_2(d)$ allows to choose independently Y_c, G_c, and l.

To get a better insight on the potential, we write the Karush–Kuhn–Tucker (KKT) conditions associated to the optimization. We define the dual quantities to the strain and damage by taking the derivative of f_{se}. We get the stress σ and a variable associated to damage denoted μ (damage criterion)

$$\sigma = (1-d)^2 E\epsilon \tag{30}$$

$$\mu = -(1-d)E\epsilon^2 + Y_c h'(d), \tag{31}$$

where $h'(d)$ denotes the derivative of h with respect to d. The KKT conditions read

$$\mu - \lambda_1 + \lambda_2 = 0 \tag{32}$$

$$\lambda_1 \ge 0, \quad d - d_n \ge 0, \quad \lambda_1(d - d_n) = 0 \tag{33}$$

$$\lambda_2 \ge 0, \quad 1 - d \ge 0, \quad \lambda_2(1-d) = 0, \tag{34}$$

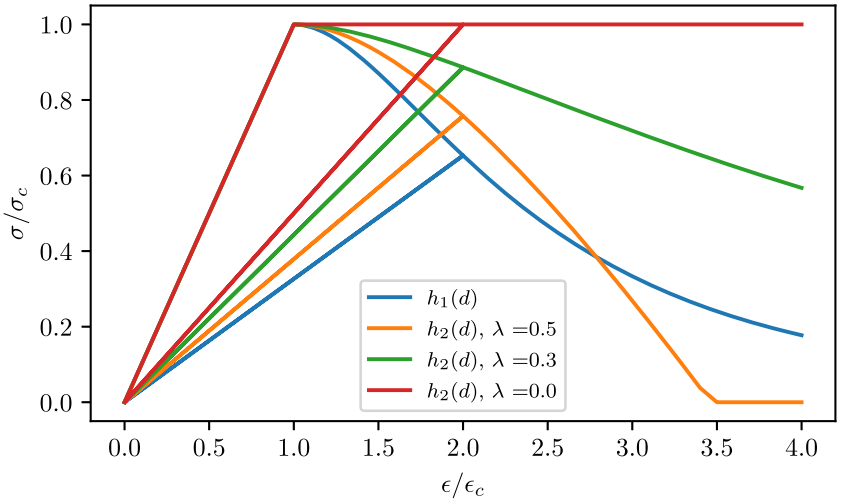

Figure 3. Stress–strain relations for the softening elastic model ($\sigma_c = \sqrt{2EY_c}, \epsilon_c = \sigma_c/E$). The strain loading/unloading follows the peak values sequence $\epsilon/\epsilon_c = (0,2,0,4)$.

where λ_1 and λ_2 are Lagrange multipliers associated to the constraints. We note that $\mu = 0$ when damage is growing (and stays below 1), and $\mu \geq 0$ when damage does not grow (and is different from 1). Figure 3 shows the stress–strain relation for a strain loading–unloading history.

The minimization of F_{se} under the constraint $(u,d) \in U_n \times D_n$ is not a convex problem. But, the minimization of F_{se} with respect to $u \in U_n$, for $d \in D_n$ fixed is a convex problem. The minimization of F_{se} with respect to $d \in D_n$ for $u \in U_n$ fixed is also a convex problem. Finally, note that in the presentation above, we did not care in presenting separately the free energy and dissipation potentials. This is not essential since we are not studying the temperature evolution. Moreover, for a given stress–strain relation this choice is in general non-unique.

4.2. *Softening elasticity with hardening plasticity*

The introduction of softening in elasto-plastic models is a complex topic. The goal here is not to find the appropriate model for a given situation but rather to discuss how the Lip-field approach is behaving in the presence of plastic internal variables. We consider a basic von Mises plasticity model with elastic softening and, in the next section, a softening plasticity model with preserved elasticity. The incremental potential for a von Mises isotropic hardening plasticity model is

$$F_p(u,\epsilon_p,p) = \int_0^L f_p(\epsilon(u),\epsilon_p,p)\,\mathrm{d}x, \quad f_p(\epsilon(u),\epsilon_p,p) = \frac{1}{2}E(\epsilon(u)-\epsilon_p)^2 + \sigma_y\left(p + \frac{k}{2}p^2\right), \tag{35}$$

where σ_y is the yield stress and k the isotropic hardening parameter. Regarding the constraints, plasticity internal variables must belong to the following convex set

$$A_n = \{(\epsilon_p,p) \in (L^\infty([0,L]))^2 : p - p_n \geq |\epsilon_p - \epsilon_{pn}|\}. \tag{36}$$

The minimization of F_{sp} with respect to $(u,(\epsilon_p,p)) \in U_n \times A_n$ is a convex problem. We introduce damage with a multiplicative approach, also called effective stress approach

$$F_{\text{sep}}(u,\epsilon_p,p,d) = \int_0^L f_{\text{sep}}(\epsilon(u),\epsilon_p,p,d)\,\mathrm{d}x, \tag{37}$$

$$f_{\text{sep}}(\epsilon(u),\epsilon_p,p,d) = (1-d)^2 f_p(\epsilon(u),\epsilon_p,p) + Y_c h(d). \tag{38}$$

The damage must belong to the set D_n defined in (26).

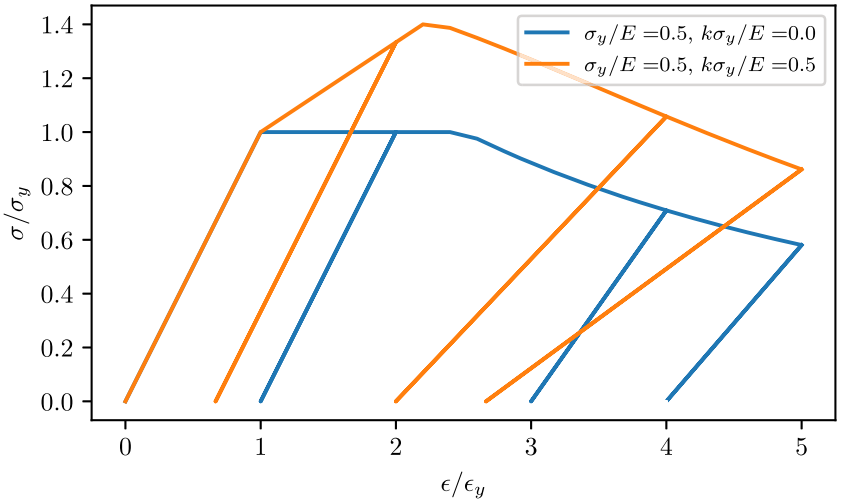

Figure 4. Stress–strain relations for the softening elasticity model with hardening plasticity with the choice $\epsilon_c/\epsilon_y = 2$, where $\epsilon_y = \sigma_y/E$. The strain loading/unloading follows the peak value sequence $\epsilon/\epsilon_y = (0, 2, e_1, 4, e_2, 5, e_3)$, where e_1, e_2, e_3 indicate the strain needed to reach full unloading ($\sigma = 0$).

Taking the derivative of f_{sep} with respect to the plastic strain, cumulative plasticity, and damage gives the stress, current yield stress, and the damage criterion, respectively.

$$\sigma = (1-d)^2 E(\epsilon - \epsilon_p) \tag{39}$$
$$R = \sigma_y (1-d)^2 (1 + kp) \tag{40}$$
$$\mu = -(1-d)E(\epsilon(u) - \epsilon_p)^2 - 2(1-d)\sigma_y(p + kp^2/2) + Y_c h'(d). \tag{41}$$

They are involved in the KKT conditions

$$\sigma + \lambda_p s(\epsilon_p - \epsilon_{pn}) = 0 \tag{42}$$
$$R - \lambda_p = 0 \tag{43}$$
$$\lambda_p \geq 0, \quad p - p_n - |\epsilon_p - \epsilon_{pn}| \geq 0, \quad \lambda_p(p - p_n - |\epsilon_p - \epsilon_{pn}|) = 0 \tag{44}$$

where s is the multi-valued signed function ($s(x) = -1$ if $x < 0$, $s(x) = +1$ if $x > 0$ and $s(0) \in [-1, 1]$). We observe that the effective stress $\sigma/(1-d)^2$ and variables ϵ_p and p may be computed from the strain independently of the damage variable. Stress–strain relations for a strain loading–unloading history are shown in Figure 4. The effect of damage may be observed in the unloading phase.

4.3. *Softening plasticity*

Finally, we consider an elasto-plastic model in which the softening affects only the yield stress leaving elasticity unchanged

$$F_{\text{sp}}(u, \epsilon_p, p, d) = \int_0^L f_{\text{sp}}(\epsilon(u), \epsilon_p, p, d)\, \mathrm{d}x,$$
$$f_{\text{sp}}(\epsilon(u), \epsilon_p, p, d) = \tfrac{1}{2} E(\epsilon(u) - \epsilon_p)^2 + (1-d)^2 \sigma_y (p + kp^2/2) + \sigma_y g(d),$$

where $g(d)$ describes softening and is chosen as $g(d) = d^2$.

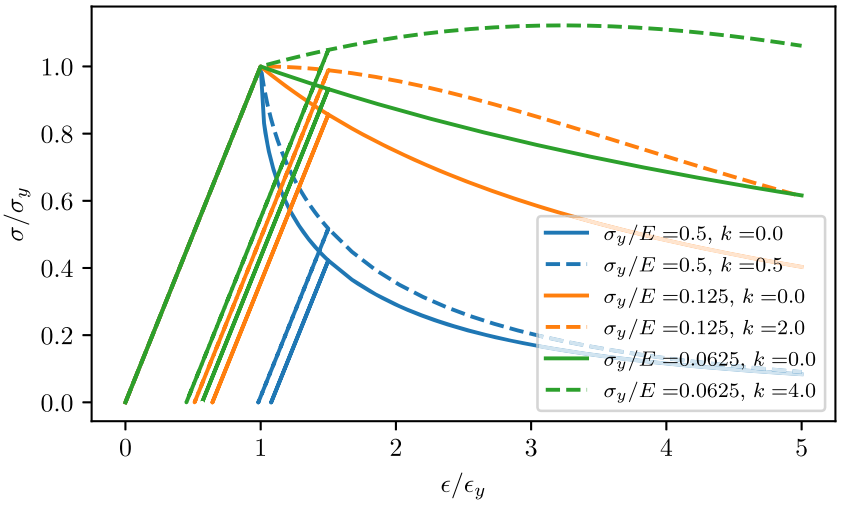

Figure 5. Stress–strain relations for the softening plastic model ($\epsilon_y = \sigma_y/E$). The strain loading/unloading follows the peak value sequence $\epsilon/\epsilon_y = (0, 1.5, e, 5)$, where e indicates the value needed to reach $\sigma = 0$.

Taking the derivative of f_{sp}, we get

$$\sigma = E(\epsilon - \epsilon_p) \tag{45}$$
$$R = \sigma_y(1-d)^2(1+kp) \tag{46}$$
$$\mu = -2\sigma_y(1-d)(p+kp^2/2) + \sigma_y g'(d), \tag{47}$$

and the associated KKT conditions

$$\sigma + \lambda_p s(\epsilon_p - \epsilon_{pn}) = 0 \tag{48}$$
$$R - \lambda_p = 0 \tag{49}$$
$$\lambda_p \geq 0, \quad p - p_n - |\epsilon_p - \epsilon_{pn}| \geq 0, \quad \lambda_p(p - p_n - |\epsilon_p - \epsilon_{pn}|) = 0. \tag{50}$$

We have omitted above the equations associated to d. They are identical to the ones presented in (32)–(34). The growth of d is now linked to cumulative plastic strain and no longer to the elastic strain (as indicated by the difference between (41) and (47)). Stress–strain relations for a strain loading–unloading history are shown in Figure 5. The elasticity is not affected as can be observed from the unloading phase.

5. Lipschitz regularization over a bar

The bar is discretized with N finite elements of equal size $h = L/N$. The displacement is linear over each element between nodal values. The internal variables are stored at each element centroid (element integration point) as indicated in Figure 6. The i index is used either for the element numbering ($d_i, i = 1, \ldots, N$ denote the damage at the centroid of each element) or for the node numbering ($u_i, i = 1, \ldots, N+1$ are the nodal displacements). The Lipschitz constraint implies the following inequalities defining the set L

$$d_i - d_{i+1} - h/l \leq 0, \quad i = 1, \ldots, N-1$$
$$d_i - d_{i-1} - h/l \leq 0, \quad i = 2, \ldots, N.$$

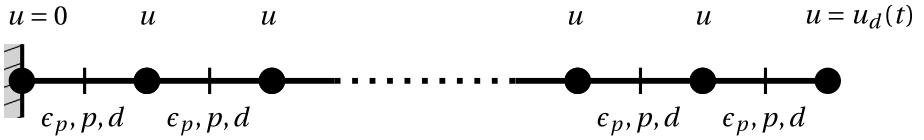

Figure 6. A one-dimensional bar discretized with equal-sized finite elements. Displacements are stored at the node, whereas internal variables are stored at the element integration point (depicted with a vertical bar).

The optimization problem reads for the softening elasticity problem

$$\min_{\substack{\boldsymbol{u}\in U_n \\ d\in D_n\cap L}} \sum_{i=1}^{N} h f_{\text{se}}\Big(\frac{u_{i+1}-u_i}{h}, d_i\Big), \tag{51}$$

and

$$\min_{\substack{(\boldsymbol{u},(\epsilon_p,p))\in U_n\times A_n \\ d\in D_n\cap L}} \sum_{i=1}^{N} h f_{\text{x}}\Big(\frac{u_{i+1}-u_i}{h}, \epsilon_{pi}, p_i, d_i\Big) \tag{52}$$

for the plasticity models (x stands for sep or sp). The set U_n enforces that $u_0 = 0$ and $u_{N+1} = u_d(t_{n+1})$. The set A_n is related to (36) and the set D_n enforces the fact that d_i must be above its previous time-step value and below 1. For all examples treated, the softening elasticity function is chosen as h_2.

The optimization problems above are solved by alternate minimization as explained in Section 3. The minimization with respect to the damage variable is performed using the scipy python library. More precisely, the scipy.optimize.minimize function is used. It is described in [49]. It offers an interface to the sequential least square quadratic programming (SLSQP) routine created by Dieter Kraft in [50].

Because of its homogeneity, the optimization problem at stake has no unique global minimizer and many local minimizers. Aware of this situation, we trigger localization by introducing a slightly higher damage on top of d_n in the middle of the bar at each step. This is just an initial guess for the alternate minimization. This strategy does not require to alter the stiffness or initial damage on the bar.

For the elastic softening model, Figure 7 gives the bar response for the non-regularized and Lip-field models. The regularizing effect of the latter is clear. Note that the case of two nodes for the discretization (a single element) gives the homogeneous bar response. No snap-back appears in this example because the regularization length is pretty large. A smaller length and toughness are used for Figure 8, and a snap-back may be observed. To handle the snap-back in the simulation, the displacement at the end of the bar is no longer imposed but controlled by limiting the strain increment over the bar at each time step. More evolved control could be used [51, 52]. Figure 8 shows the non-regularized case (left column), a convergence toward a solution without any dissipation (zero areas under the converged curve). On the contrary, the converged solution (right column) indicates a non-zero dissipation (whose dimensional value is close to the toughness G_c).

Still, for the elastic softening model, we show, Figure 9, that the stress–strain response does not vary much with the regularization length (demonstrating the nice capability of the h_2 softening function). The response are obtained for a non-varying toughness, G_c, and strength Y_c. Only the regularization length is varied (and the mesh size is adjusted to always have the same number of elements over l). We observe a dimensional area under the curve close to G_c.

Regarding the softening elastic model with hardening plasticity, the response is given in Figure 10 (left column). We observe that plasticity proceeds first in an homogeneous fashion, without any damage. During this homogeneous phase, the stress–average strain curve is rising.

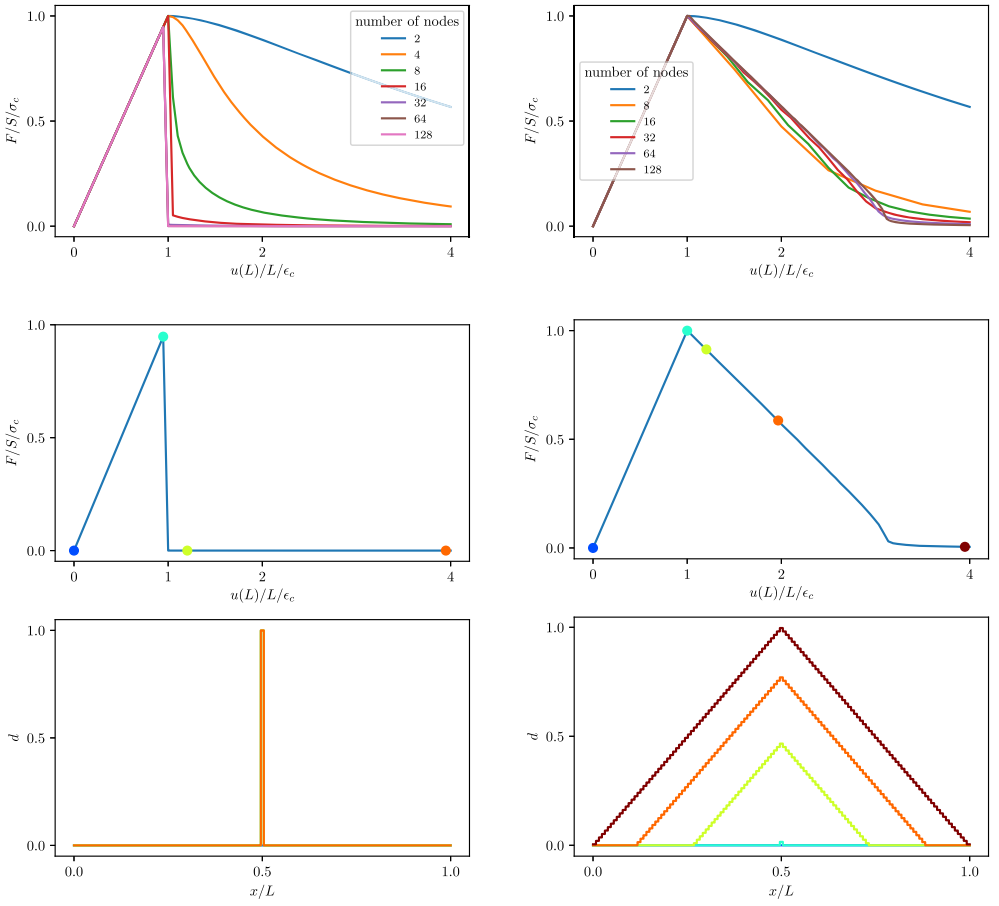

Figure 7. Response for the bar with the elastic softening behavior and imposed displacement: non-regularized model (left) and Lip-field model (right). The top row gives the stress–strain average response, and the bottom one the damage profile at the color dots given in the middle row. The mesh used for the middle row is the most refined of the top row. Parameters are: $L = 1$, $l = 0.5$, $E = 1$, $Y_c = 1$, $\lambda = 0.3$, $G_c = 10/3$.

As this curve reaches its peak, localization of the damage and plasticity starts to occur. For the softening plasticity model, the response is given in Figure 10 (right column). We observe that plasticity and damage proceed first in an homogeneous manner due to the initial hardening effect of plasticity, then concentrates. The departure from the homogeneous response also occurs when the stress–average strain reaches its limit point.

We provide a last example with a non-uniform loading caused by a volumic force $f(x/L) = 0.1 * \sin(8 * \pi * x/L)$. This loading is added to the imposed displacement. The results are depicted in Figure 11. The model parameters are the same as for Figure 10 (right column) except that $l = 0.25$ and the number of nodes is 256. The damage develops in a complex pattern. The right column gives the results for the non-regularized case (local approach $l = 0$). We observe the Lip-field results (right column) are the same as the local approach as long as the stress–average strain curve did not reach the peak point. This demonstrates the fact that the Lip-field approach preserves the local solution when it is not localizing. This is quite different from the other regularizing approaches (non-local, damage gradient, phase-field) that will modify the local solution even prior to localization. It may also be seen from Figure 11 that the normal derivative of the damage

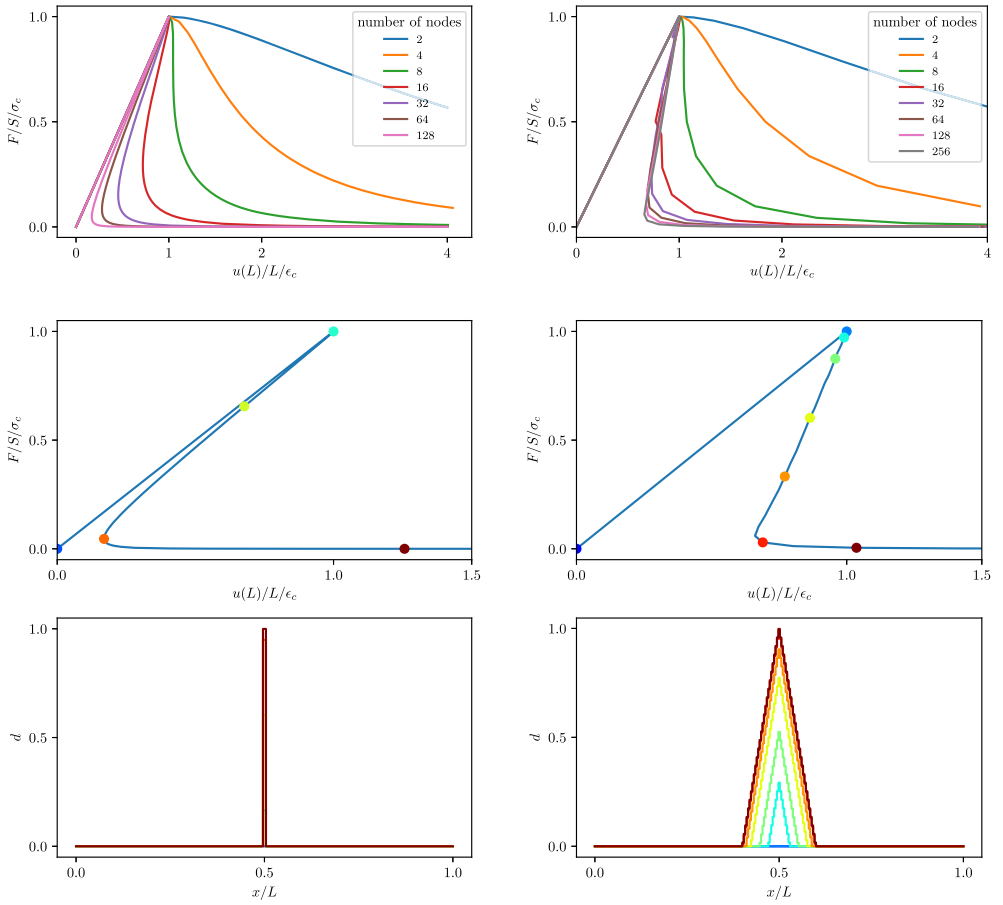

Figure 8. Response for the bar with the elastic softening behavior and snap-back control: non-regularized model (left) and Lip-field model (right), convergence of the stress–average strain response (top) and damage evolution (bottom) corresponding the color dots in the middle figures. The middle figures reproduce the curve of the top figures for the most refined grid. Parameters are: $L = 1$, $l = 0.1$, $E = 1$, $Y_c = 1$, $\lambda = 0.3$, $G_c = 2/3$.

is not zero at the boundary, as it would have been the case for damage gradient-based models. The Lipschitz constraint does not enforce a given value for the normal derivative of the damage on the boundary but just bounds the value.

6. Conclusion and future works

A new regularization approach has been introduced to alleviate spurious localization with softening material models. Both elastic and plastic softening models have been considered. The regularization enforces a Lipschitz condition on the field responsible for the softening. In doing so, a length is introduced in the model.

Compared to the gradient damage or phase-field approaches, the Lip-field approach introduces an extra constraint but does not affect the expression of the incremental potential (the objective function in the minimization is not modified). In other words, the energy does not depend on the damage gradient but solely on the damage. Its expression is the one of the local model. As a

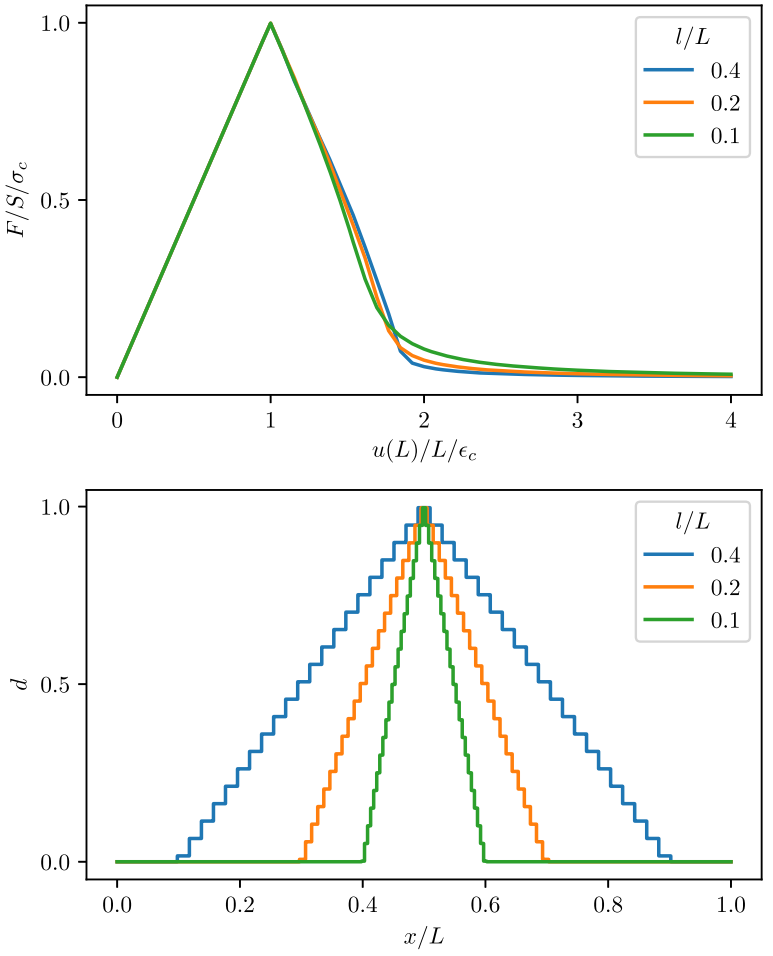

Figure 9. Lip-field model response with the elastic softening behavior (choice h_2) for several regularization length values. Stress–average strain response (above) and damage profile (below). Parameters are: $L = 1.$, $l = (0.4, 0.2, 0.1)$, $E = 1.$, $Y_c = 1.$, $\lambda = (0.4, 0.2, 0.1)$, $G_c = 2$. The number of elements is 51, 101, and 201 so that we have $h/l \sim 20$.

consequence, the Lip-field does not introduce an extra partial differential equation with its questionable boundary conditions. From a mathematical point of view, the Lipschitz constraint may be interpreted as searching the damage field among subsolutions (in the viscosity sense) of the eikonal equation [53, 54] or as viscosity solutions to an eikonal inequality.

Compared to the non-local integral approach, no widening of the fully damage zone is observed and the implementation only requires an element to be related to its neighbors. Finally, compared to the thick level set approach, the level set know-how is no longer needed.

Future works will be dedicated to the extension of the results to two- and three-dimensional problems. For this extension, the bounds demonstrated in this paper (valid for any dimensions) will allow one to predict a priori the zones over which damage is affected by the Lipschitz constraint. This will reduce the cost of the damage optimization.

Finally, the paper did not discuss the possibility of allowing displacement jumps during the simulation. This issue is important when dealing with fragmentation or crack under large deformation and needs to be studied in the future for the Lip-field approach.

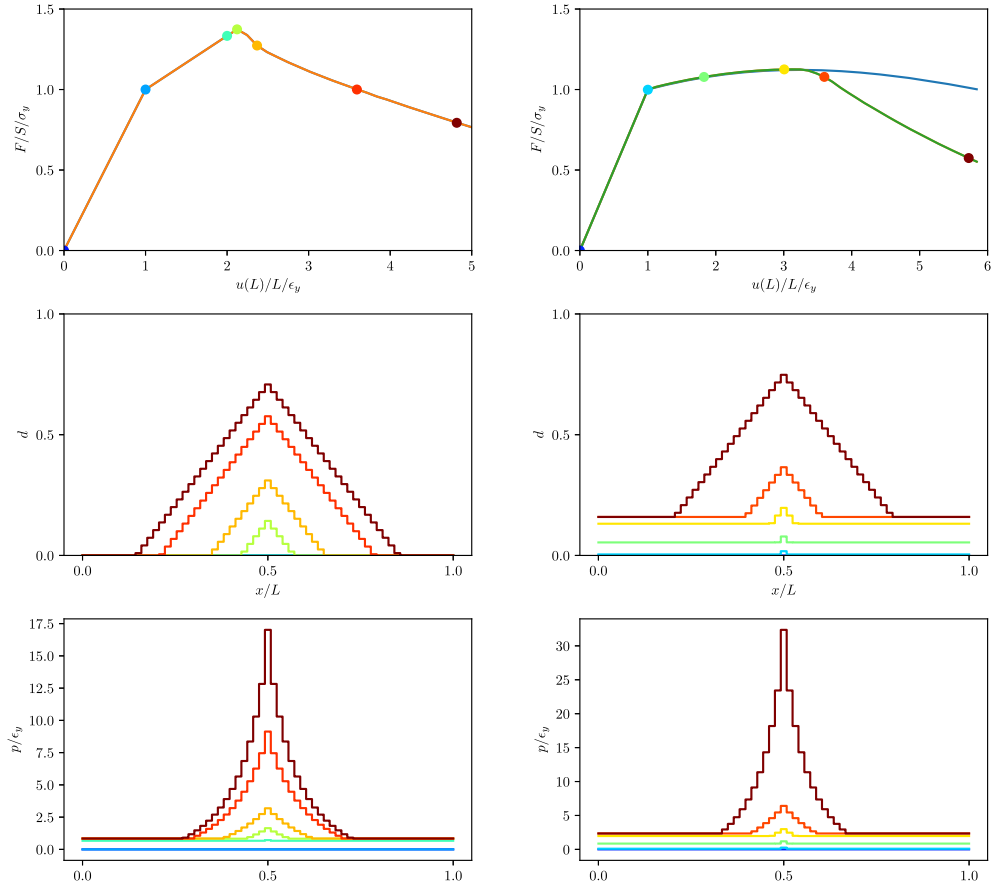

Figure 10. Lip-field model response for the softening elasticity model with plasticity hardening (left column) and softening plasticity (right column): stress–strain average curves (top row), damage field (middle row), and cumulative plasticity (bottom row). For both models, $L = 1$, $l = 0.5$, and the mesh size is $h = L/64$. Model specific parameters are: $E = 2$, $\sigma_y = 1$, $Y_c = 1$, $k = 1$, $\lambda = 1/3$ for the hardening plasticity (corresponding to the model the orange curve in Figure 4) and $E = 1.$, $\sigma_y = 1/16$, $k = 4$ for the softening plasticity model (corresponding to the model with the dashed green curve in Figure 5).

Acknowledgments

The authors wish to thank J. Dolbow, B. Le, B. Masseron, G. Rastiello, J. Rethore, A. Salzman, I. Stefanou, A. Stershic, and C. Stolz for their advice on ways to improve the manuscript.

Appendix A. Proof of the bounds

Consider a field d defined over Ω. To this field, we associate two other fields denoted $\pi^{\mathrm{u}} d$ and $\pi^{\mathrm{l}} d$, called upper and lower projections, respectively.

$$\pi^{\mathrm{u}} : L^\infty(\Omega) \mapsto L : d(\boldsymbol{x}) \mapsto \pi^{\mathrm{u}} d(\boldsymbol{x}) = \max_{\boldsymbol{y}\in\Omega} \left(d(\boldsymbol{y}) - \frac{1}{l}\mathrm{dist}(\boldsymbol{x},\boldsymbol{y}) \right), \tag{53}$$

$$\pi^{\mathrm{l}} : L^\infty(\Omega) \mapsto L : d(\boldsymbol{x}) \mapsto \pi^{\mathrm{l}} d(\boldsymbol{x}) = \min_{\boldsymbol{y}\in\Omega} \left(d(\boldsymbol{y}) + \frac{1}{l}\mathrm{dist}(\boldsymbol{x},\boldsymbol{y}) \right). \tag{54}$$

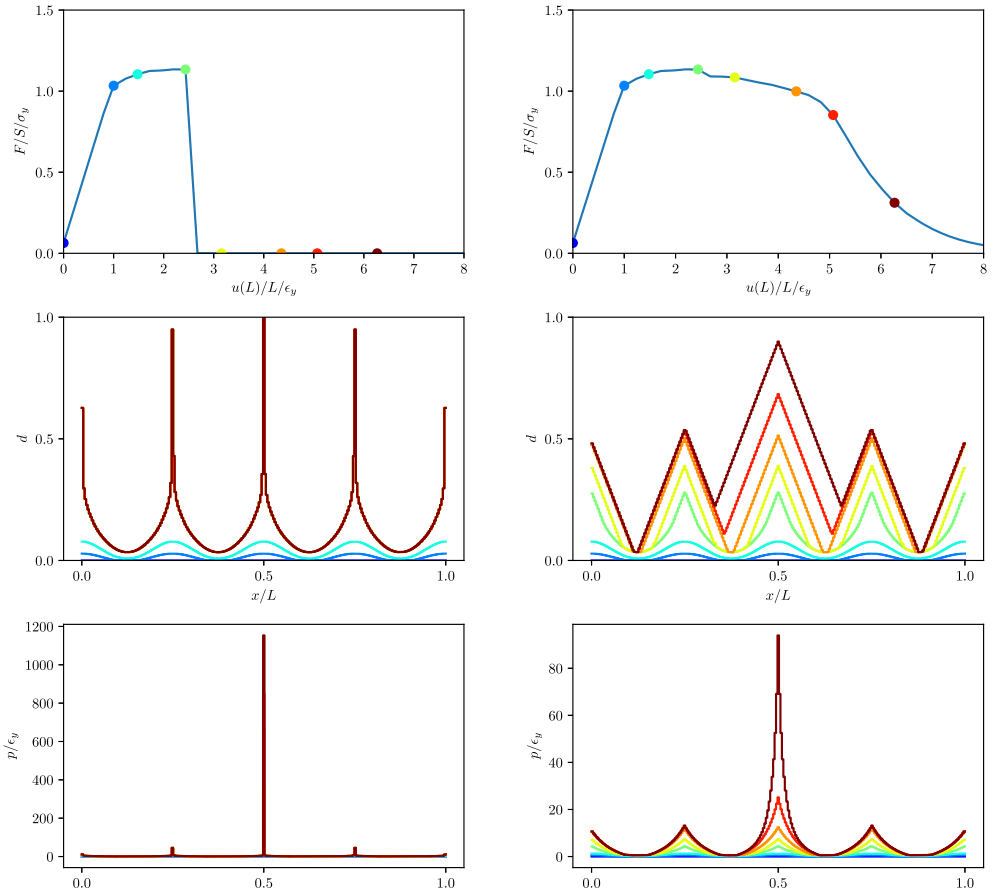

Figure 11. Response for a softening plasticity model with a volumic oscillatory force. No regularization, $l = 0$ (left) and Lip regularization (right). Stress–average strain results (top), damage (middle), and cumulative plasticity profile (bottom). Parameters are: $L = 1$, $l = 0.25$, $h = 1/255$, $E = 1$, $\sigma_y = 1/16$, $k = 4$.

They satisfy the following properties:

(a) $\pi^{\mathrm{l}} d \in L$, $\pi^{\mathrm{u}} d \in L$
(b) $d \in L \Rightarrow \pi^{\mathrm{l}} d = \pi^{\mathrm{u}} d = d$
(c) $\pi^{\mathrm{l}} d \le d \le \pi^{\mathrm{u}} d$
(d) $d_1 \le d_2 \Rightarrow \pi^{\mathrm{l}} d_1 \le \pi^{\mathrm{l}} d_2$, $\pi^{\mathrm{u}} d_1 \le \pi^{\mathrm{u}} d_2$ (monotonicity)

To prove that the mapping falls indeed in L (property (a)), we take the difference

$$\pi^{\mathrm{u}} d(\boldsymbol{x}^1) - \pi^{\mathrm{u}} d(\boldsymbol{x}^2) = \max_{\boldsymbol{y}\in\Omega} \left(d(\boldsymbol{y}) - \frac{1}{l}\mathrm{dist}(\boldsymbol{x}^1, \boldsymbol{y}) \right) - \max_{\boldsymbol{y}\in\Omega} \left(d(\boldsymbol{y}) - \frac{1}{l}\mathrm{dist}(\boldsymbol{x}^2, \boldsymbol{y}) \right). \tag{55}$$

Using the triangular inequality written as

$$\mathrm{dist}(\boldsymbol{x}^1, \boldsymbol{y}) \le \mathrm{dist}(\boldsymbol{x}^1, \boldsymbol{x}^2) + \mathrm{dist}(\boldsymbol{x}^2, \boldsymbol{y})$$

we get

$$\pi^{\mathrm{u}} d(\boldsymbol{x}^1) - \pi^{\mathrm{u}} d(\boldsymbol{x}^2) \ge -\frac{1}{l}\mathrm{dist}(\boldsymbol{x}^1, \boldsymbol{x}^2),$$

and using the triangular inequality as

$$\operatorname{dist}(\boldsymbol{x}^2,\boldsymbol{y}) \leq \operatorname{dist}(\boldsymbol{x}^2,\boldsymbol{x}^1) + \operatorname{dist}(\boldsymbol{x}^1,\boldsymbol{y})$$

we get

$$\pi^{\mathrm{u}} d(\boldsymbol{x}^1) - \pi^{\mathrm{u}} d(\boldsymbol{x}^2) \leq \frac{1}{l}\operatorname{dist}(\boldsymbol{x}^1,\boldsymbol{x}^2).$$

The proof is similar for $\pi^{\mathrm{l}} d$. Property (b) is obtained from the definition of $d \in L$:

$$d(\boldsymbol{y}) - \frac{1}{l}\operatorname{dist}(\boldsymbol{x},\boldsymbol{y}) \leq d(\boldsymbol{x}) \leq d(\boldsymbol{y}) + \frac{1}{l}\operatorname{dist}(\boldsymbol{x},\boldsymbol{y}). \tag{56}$$

Computing the minimum and maximum over $\boldsymbol{y}$ for the upper and lower bounds, respectively, yields the property. Property (c) is obtained directly from the definition of the projections by testing $\boldsymbol{y}$ as $\boldsymbol{x}$ in the max and min. Similarly, property (d) stems from the definition of the projections.

We now discuss the consequences of the properties. Properties (a) and (b) indicate that the projections are idempotent (applied twice yield the same result as applied once). Property (c) indicates that at any point where the projections are equal, they are equal to d. Combining properties (c) and (d) and using the fact that $d_n \in L$ (as well as noting that any uniform function is Lipschitz) yield the result (21).

We are now ready to prove the bounds result (22). Consider a damage field $d^* \in D_n \cap L$ lying outside the bounds, we associate to this field another field by clipping it to the bounds

$$d^{**}(\boldsymbol{x}) = \max(\pi^{\mathrm{l}}\overline{d}(\boldsymbol{x}), \min(d^*(\boldsymbol{x}), \pi^{\mathrm{u}}\overline{d}(\boldsymbol{x}))). \tag{57}$$

Since the minimum of Lipschitz functions (with the same constant) is also Lipschitz (and similarly for maximum), the field d^{**} belongs also to $D_n \cap L$. The field d^{**} is a better solution than d^* because it lowers the objective function

$$F(d^{**}) \leq F(d^*). \tag{58}$$

Indeed, the objective function F is an integral over Ω of a convex local function with respect to d denoted by f, and we show that the inequality also holds at the local level

$$f(d^{**}) \leq f(d^*). \tag{59}$$

We have two possible orderings

$$d^* < d^{**} = \pi^{\mathrm{l}}\overline{d} \leq \overline{d} \quad \text{or} \quad \overline{d} \leq \pi^{\mathrm{u}}\overline{d} = d^{**} < d^*. \tag{60}$$

So, there exist $\lambda \in]0,1[$ such that

$$d^{**} = \lambda\overline{d} + (1-\lambda)d^* \tag{61}$$

leading to, by strict convexity of f

$$f(d^{**}) < \lambda f(\overline{d}) + (1-\lambda) f(d^*) = f(d^*) + \lambda(f(\overline{d}) - f(d^*)) < f(d^*), \tag{62}$$

where the last inequality is obtained from the fact that $\overline{d}$ at $\boldsymbol{x}$ is the minimum of f at $\boldsymbol{x}$. Thus, to any field satisfying the constraints but lying outside the bounds, we can associate a better one inside the bounds, it proves that the optimal solution is inside the bounds.

Appendix B. Nonlinear solver

The nonlinear solver used for (16) alternates between a local and global step. The m exponent is used to denote these iterations. The local step computes at each integration point the stress σ^m and internal variables ϵ_p^m, p^m, as well as the tangent operator T^m knowing u^m, ϵ_p^n, p^n, and d^k. The n exponent indicates the previous known time-step values, whereas the k exponent indicates the latest computed value of damage from (17) in the alternate minimization.

The global step involves a linear solve which finds $u^{m+1} \in U_n$ such that

$$\int_0^L T^m \epsilon(u^{m+1} - u^m)\epsilon(u^*)\,\mathrm{d}x = -\int_0^L \sigma^m \epsilon(u^*)\,\mathrm{d}x,\ \forall u^* \in U_0.$$

When the correction $u^{m+1} - u^m$ is below a threshold, we set $u^{k+1}, \epsilon_p^{k+1}, p^{k+1}$ as the current m values. The expressions of σ^m and T^m are given below for each model.

B.1. *Softening elasticity*

We have

$$\sigma^m = (1-d^k)^2 E\epsilon^m, \quad \epsilon^m = \epsilon(u^m), \quad T^m = (1-d^k)^2 E. \tag{63}$$

Since the model is linear, a single "m" iteration is needed to converge. If dissymmetric tension–compression behavior was considered for damage, more iterations would be needed to converge.

B.2. *Softening elasticity with hardening plasticity*

The trial stress is computed as

$$\sigma^t = E(1-d^k)^2(\epsilon^m - \epsilon_p^n)$$

followed by the plasticity criterion

$$f^t = |\sigma^t| - \sigma_y(1-d^k)^2(1+kp^n)$$

giving two cases

$$\begin{aligned}
&\text{if } f^t <= 0 \quad \epsilon_p^m = \epsilon_p^n,\ p^m = p^n,\ \sigma^m = \sigma^t, T^m = E(1-d^k)^2\\
&\text{if } f^t > 0 \quad p^m = \frac{|\sigma^t| - \sigma_y + Ep^n}{E+\sigma_y k}, \quad T^m = \frac{E\sigma_y k(1-d^k)^2}{E+\sigma_y k}\\
&\epsilon_p^m = \epsilon_p^n + (p^m - p^n)\frac{\sigma^t}{|\sigma^t|}, \quad \sigma^m = E(1-d^k)^2(\epsilon^m - \epsilon_p^m).
\end{aligned}$$

B.3. *Softening plasticity*

The trial stress is computed as

$$\sigma^t = E(\epsilon^m - \epsilon_p^n)$$

followed by the plasticity criterion

$$f^t = |\sigma^t| - \sigma_y(1-d^k)^2(1+kp^n)$$

and two cases

$$\begin{aligned}
&\text{if } f^t <= 0: \quad \epsilon_p^m = \epsilon_p^n,\ p^m = p^n,\ \sigma^m = \sigma^t,\ T^m = E\\
&\text{if } f^t > 0: \quad p^m = \frac{|\sigma^t| - \sigma_y(1-d^k)^2 + Ep^n}{E+\sigma_y k(1-d^k)^2}, \quad T^m = \frac{E\sigma_y k(1-d^k)^2}{E+\sigma_y k(1-d^k)^2}\\
&\epsilon_p^m = \epsilon_p^n + (p^m - p^n)\frac{\sigma^t}{|\sigma^t|}, \quad \sigma^m = E(\epsilon^m - \epsilon_p^m).
\end{aligned}$$

References

[1] Z. Bazant, T. Belytschko, T. Chang, "Continuum theory fo strain-softening", *J. Eng. Mech.* **110** (1984), p. 1666-1692.

[2] G. Pijaudier-Cabot, Z. Bazant, "Non-local damage theory", *J. Eng. Mech.* **113** (1987), p. 1512-1533.

[3] Z. Bazant, M. Jirasek, "Nonlocal integral formulations of plasticity and damage: survey of progress", *J. Eng. Mech.* **128** (2002), p. 1119-1149.

[4] E. Lorentz, S. Andrieux, "Analysis of non-local models through energetic formulations", *Int. J. Solids Struct.* **40** (2003), p. 2905-2936.

[5] C. Giry, F. Dufour, J. Mazars, "International journal of solids and structures stress-based nonlocal damage model", *Int. J. Solids Struct.* **48** (2011), no. 25–26, p. 3431-3443.

[6] G. Rastiello, C. Giry, F. Gatuingt, R. Desmorat, "From diffuse damage to strain localization from an Eikonal Non-Local (ENL) Continuum Damage model with evolving internal length", *Comput. Methods Appl. Mech. Eng.* **331** (2018), p. 650-674.

[7] E. C. Aifantis, "On the microstructural origin of certain inelastic models", *J. Eng. Mater. Technol.* **106** (1984), no. 4, p. 326-330.

[8] A. E. Triantafyllidis N, "A gradient approach to localization of deformation: I. Hyperelastic model", *J. Elast.* **16** (1986), p. 225-237.

[9] C. Z. Schreyer H, "One-dimensional softening with localization", *J. Appl. Mech.* **53** (1986), p. 891-979.

[10] H. B. Mühlhaus, L. Vardoulakis, "The thickness of shear bands in granular materials", *Geotechnique* **37** (1987), p. 271-283.

[11] M. Frémond, B. Nedjar, "Damage, gradient of damage and principle of virtual power", *Int. J. Solids Struct.* **33** (1996), no. 8, p. 1083-1103.

[12] G. Pijaudier-Cabot, N. Burlion, "Damage and localisation in elastic materials with voids", *Mech. Cohesive-Frict. Mater.* **144** (1996), p. 129-144.

[13] R. Peerlings, M. Geers, R. De Borst, W. Brekelmans, "A critical comparison of nonlocal and gradient-enhanced softening continua", *Int. J. Solids Struct.* **38** (2001), no. 44–45, p. 7723-7746.

[14] Q.-S. Nguyen, S. Andrieux, "The non-local generalized standard approach: a consistent gradient theory", *C. R. Acad. Sci.: Méc., Phys., Chim., Astronom.* **333** (2005), p. 139-145.

[15] D. Mumford, J. Shah, "Optimal approximations by piecewise smooth functions and associated variational problems", *Commun. Pure Appl. Math.* **42** (1989), p. 577-685.

[16] L. Ambrosio, "Existence theory for a new class of variational problems", *Arch. Ration. Mech. Anal.* **111** (1990), p. 291-322.

[17] L. Ambrosio, A. Braides, "Energies in SBV and variational models in fracture mechanics", in *Proceedings of the EurHomogenization Congress, Nizza, Gakuto Int. Series, Math. Sci. and Appl.*, 1997, p. 1-22.

[18] L. Ambrosio, V. Tortorelli, "Approximation of functionals depending on jumps by elliptic functionals via gamma-convergence", *Commun. Pure Appl. Math.* **43** (1990), p. 999-1036.

[19] E. De Giorgi, "New problems on minimizing movements", in *Boundary Value Problems for PDE and Applications* (C. Baiocchi, J. Lions, eds.), Masson, Paris, 1993, p. 81-98.

[20] M. Buliga, "Energy minimizing brittle crack propagation", *J. Elast.* **52** (1998), no. 3, p. 201-238.

[21] M. Buliga, "Hamiltonian inclusions with convex dissipation with a view towards applications", *Ann. Acad. Romanian Sci.: Ser. Math. Appl.* **1** (2009), no. 2, p. 228-251.

[22] B. Bourdin, G. A. Francfort, J.-J. Marigo, "Numerical experiments in revisited brittle fracture", *J. Mech. Phys. Solids* **48** (2000), no. 4, p. 797-826.

[23] G. A. Francfort, J.-J. Marigo, "Revisiting brittle fracture as an energy minimization problem", *J. Mech. Phys. Solids* **46** (1998), p. 1319-1412.

[24] A. Mielke, *Evolution in Rate-Independent Systems*, Elsevier, B.V., Amsterdam, 2005, Chap. 6, 461-559 pages.

[25] B. Bourdin, G. a. Francfort, J.-J. Marigo, "The variational approach to fracture", *J. Elast.* **91** (2008), no. 1–3, p. 5-148.

[26] A. Karma, D. Kessler, H. Levine, "Phase-field model of mode III dynamic fracture", *Phys. Rev. Lett.* **87** (2001), no. 4, article no. 045501.

[27] V. Hakim, A. Karma, "Laws of crack motion and phase-field models of fracture", *J. Mech. Phys. Solids* **57** (2009), no. 2, p. 342-368.

[28] H. Amor, J.-J. Marigo, C. Maurini, "Regularized formulation of the variational brittle fracture with unilateral contact: numerical experiments", *J. Mech. Phys. Solids* **57** (2009), no. 8, p. 1209-1229.

[29] C. Miehe, F. Welschinger, M. Hofacker, "Thermodynamically consistent phase-field models of fracture: variational principles and multi-field FE implementations", *Int. J. Numer. Methods Eng.* **83** (2010), no. 10, p. 1273-1311.

[30] C. Miehe, M. Hofacker, F. Welschinger, "A phase field model for rate-independent crack propagation: robust algorithmic implementation based on operator splits", *Comput. Methods Appl. Mech. Eng.* **199** (2010), no. 45–48, p. 2765-2778.

[31] C. Kuhn, R. Müller, "A continuum phase field model for fracture", *Eng. Fract. Mech.* **77** (2010), no. 18, p. 3625-3634.

[32] M. Ambati, T. Gerasimov, L. De Lorenzis, "Phase-field modeling of ductile fracture", *Comput. Mech.* **55** (2015), no. 5, p. 1017-1040.
[33] N. Moës, C. Stolz, P.-E. Bernard, N. Chevaugeon, "A level set based model for damage growth: the thick level set approach", *Int. J. Numer. Methods Eng.* **86** (2011), p. 358-380.
[34] C. Stolz, N. Moës, "A new model of damage: a moving thick layer approach", *Int. J. Fract.* **174** (2012), no. 1, p. 49-60.
[35] N. Moës, C. Stolz, N. Chevaugeon, "Coupling local and non-local damage evolution with The Thick Level Set model", *Adv. Model. Simul. Eng. Sci.* **2** (2014), no. 16, p. 1-21.
[36] A. J. Stershic, J. E. Dolbow, N. Moës, "The Thick Level-Set Model for dynamic fragmentation", *Eng. Fract. Mech.* **172** (2017), p. 39-60.
[37] M. Frémond, C. Stolz, "On alternative approaches for graded damage modelling", in *Models, Simulation, and Experimental Issues in Structural Mechanics* (M. Frémond, F. Maceri, G. Vairo, eds.), Springer Series in Solid and Structural Mechanics, vol. 8, Springer International Publishing, Cham, 2017, p. 87-104.
[38] N. Valoroso, C. Stolz, "Progressive damage in quasi-brittle solids", in *Proceedings of XXIV AIMETA Conference 2019* (A. Carcaterra, A. Paolone, G. Graziani, eds.), AIMETA 2019, Springer, 2020.
[39] P. Mialon, "Eléments d'analyse et de résolution numérique des relations de l'élasto-plasticité", *Bull. Dir. Études Rech.—Electr. Fr. Sér. C Math. Informat.* (1986), no. 3, p. 57-88 (French).
[40] M. Ortiz, L. Stainier, "The variational formulation of viscoplastic constitutive updates", *Comput. Methods Appl. Mech. Eng.* **171** (1999), no. 3, p. 419-444.
[41] L. Boyd, S. P. Vandenberghe, *Convex Optimization*, Cambridge University Press, Cambridge, 2004.
[42] V. Krishnan, A. A. A. Makdah, F. Pasqualetti, "Lipschitz bounds and provably robust training by Laplacian smoothing", https://arxiv.org/abs/2006.03712, 2020.
[43] B. Halphen, Q.-S. Nguyen, "Sur les matériaux standards généralisés", *J. Méc.* **14** (1975), no. 1, p. 39-63.
[44] P. Germain, P. Suquet, Q. S. Nguyen, "Continuum thermodynamics", *ASME J. Appl. Mech.* **50** (1983), p. 1010-1020.
[45] J. Simo, T. Hughes, *Computational Inelasticity*, Springer, New York, 1997, 392 pages.
[46] J. Zghal, K. Moreau, N. Moës, D. Leguillon, C. Stolz, "Analysis of the failure at notches and cavities in quasi-brittle media using the Thick Level Set damage model and comparison with the coupled criterion", *Int. J. Fract.* **211** (2018), no. 1–2, p. 253-280.
[47] E. Lorentz, V. Godard, "Gradient damage models: toward full-scale computations", *Comput. Methods Appl. Mech. Eng.* **200** (2011), no. 21–22, p. 1927-1944.
[48] A. Parrilla Gómez, N. Moës, C. Stolz, "Comparison between thick level set (TLS) and cohesive zone models", *Adv. Model. Simul. Eng. Sci.* **2** (2015), no. 1, article no. 18.
[49] P. Virtanen *et al.*, "SciPy 1.0 Contributors, SciPy 1.0: fundamental algorithms for scientific computing in Python", *Nat. Methods* **17** (2020), p. 261-272.
[50] D. Kraft *et al.*, "A software package for sequential quadratic programming", 1988, http://hdl.handle.net/10068/147127.
[51] M. A. Crisfield, "A fast incremental/iterative solution procedure that handles "snap-through"", *Comput. Struct.* **13** (1981), p. 55-62.
[52] R. De Borst, "Computation of post-bifurcation and post-failure behavior of strain softening solids", *Comput. Struct.* **2** (1987), no. 2, p. 211-224.
[53] M. Crandall, P.-L. Lions, "Viscosity solutions of Hamilton–Jacobi equations", *Trans. Am. Math. Soc.* **277** (1983), p. 1-42.
[54] M. Crandall, L. Evans, R. Gariepy, "Optimal Lipschitz extensions and the infinity Laplacian", *Calc. Var. Partial Differ. Equ.* **13** (2001), p. 123-139.